

JGR Atmospheres

RESEARCH ARTICLE

10.1029/2025JD043690

Key Points:

- Soil moisture (SM) in northern Tibetan Plateau (TP) is sustained from spring to summer by a positive feedback with precipitation
- The SM anomaly in northern TP leads to the abnormal cyclonic circulation in the western TP through the mechanism of thermal adaptation
- SM in the northern TP may serve as a forecasting pathway for summer precipitation in the Northwest China

Correspondence to:

H. Yu,
yuhp@lzb.ac.cn

Citation:

Lu, F., Yu, H., Hu, Z., Xie, Y., Bai, D., Wang, X., et al. (2025). Effects of soil moisture in northern Tibetan Plateau on summer precipitation in Northwest China. *Journal of Geophysical Research: Atmospheres*, 130, e2025JD043690.
<https://doi.org/10.1029/2025JD043690>

Received 20 FEB 2025

Accepted 16 JUN 2025

Effects of Soil Moisture in Northern Tibetan Plateau on Summer Precipitation in Northwest China

Fuquan Lu^{1,2}, Haipeng Yu¹ , Zeyong Hu¹ , Yongkun Xie³ , Dongping Bai^{1,2}, Xin Wang⁴, Shanling Cheng^{1,2}, Haojie Wu^{1,2}, and Bofei Zhang^{1,2}

¹State Key Laboratory of Cryospheric Science and Frozen Soil Engineering, Nagqu Plateau Climate and Environment Observation and Research Station of Tibet Autonomous Region, Northwest Institute of Eco-Environment and Resources, Chinese Academy of Sciences, Lanzhou, China, ²University of Chinese Academy of Sciences, Beijing, China, ³Collaborative Innovation Center for Western Ecological Safety, Lanzhou University, Lanzhou, China, ⁴College of Earth and Environmental Sciences, Lanzhou University, Lanzhou, China

Abstract Soil moisture (SM) on the Tibetan Plateau (TP), a crucial climate variable with “memory,” influences the East Asia climate by modulating surface energy and water vapor exchanges. Understanding the relationship between TP soil moisture (TPSM) and summer precipitation in Northwest China (NWC) is essential for improving climate predictions for East Asia. However, most existing studies have focused on the connection between TPSM and the climate of East Asian monsoon region, whereas the mechanisms by which TPSM influence precipitation in NWC, a nonmonsoonal area, remain underexplored. This study investigates how spring anomalies of TPSM persist into summer and influence summer precipitation in NWC. The results indicate that anomalies in spring TPSM can initiate a positive feedback with precipitation, which affects the intensity of plateau monsoon and contributes to the persistence of SM anomaly from spring to summer. During summer, positive SM anomalies in northern TP facilitate maintaining cyclonic circulation anomalies over western TP and trigger eastward-propagating Rossby waves that induce anticyclonic circulation anomalies over eastern NWC. The anomalous circulation results in upward motion in the western NWC and subsidence in the eastern NWC enhancing precipitation in the western NWC while reducing the precipitation in the north. Finally, the findings from the circulation analysis are validated through numerical model simulations. This study provides valuable insights into the climatic effects of TPSM and offers important implications for precipitation prediction in NWC.

Plain Language Summary Soil moisture on the Tibetan Plateau, a high-altitude region in Asia, acts like a natural “memory” that influences weather patterns over time. This study explores how changes in the plateau’s soil moisture during spring can affect summer rainfall in Northwest China, a dry region far from monsoon influences. Researchers found that unusually wet or dry soil in spring can create a self-reinforcing cycle: It alters rainfall patterns, which then strengthens the soil moisture anomaly and prolongs its effects into summer. In summers with wetter-than-normal soil on the northern Tibetan Plateau, rotating wind patterns form over the plateau and send atmospheric waves eastward. These waves shift air circulation over Northwest China causing more rain in the western part of the region but less in the north. Computer simulations confirmed these connections. By revealing how soil moisture in one region can trigger distant weather changes, this research helps improve predictions of summer rainfall in dry areas of China, which is vital for managing water resources and preparing for droughts or floods. The findings also highlight the Tibetan Plateau’s role as a key driver of Asia’s climate system.

1. Introduction

The Tibetan Plateau (TP), with an average elevation exceeding 4,000 m, is the most topographically complex plateau in the world and is often referred to as the “Third Pole” of the Earth. During the summer, the TP acts as a significant heat source, directly warming the middle and upper troposphere, functioning as both a “trigger” and an “amplifier.” This substantially influences the heat exchange and energy storage/release between the TP’s surface and its surrounding atmospheric system with profound effects on global atmospheric circulation as well as regional and global weather and climate patterns (Huang et al., 2023; Kitoh, 2004; Lu et al., 2018, 2021; Wu, 1984; Wu et al., 2007, 2014; Wu, Liu et al., 2012; Xie et al., 2023; Xu et al., 2002). As a result, the thermal effects of the TP have long been a central focus in climate change and the ecological environment.

Studies have shown that the thermal effects of TP significantly influence precipitation patterns in East Asia (Duan et al., 2013; Zhang et al., 2019). The TP enhances the thermal contrast between land and ocean acting as a major heat source during the summer and strengthening the East Asian summer monsoon (Hahn & Manabe, 1975; Wu, Guan, et al., 2012; Wu & Zhang, 1998) with significant impacts on precipitation in East Asia (Shang et al., 2022; Zha & Wu, 2023; C. Zhu et al., 2023; X. Zhu et al., 2023). Soil moisture (SM) is a key indicator of the Plateau's thermal forces. By influencing surface latent heat, vegetation growth, and evaporation, TP soil moisture (TPSM) alters energy exchanges between land and atmosphere, thereby modifying the thermal state of TP and impacting the midlatitude atmospheric circulation (Wu et al., 2007). Seasonal anomalies of SM play a key role in seasonal changes in the atmosphere and significantly affect temperature and precipitation over long periods of time. Additionally, the seasonal freeze-thaw cycle of TP soil exerts a considerable influence on atmospheric circulation over TP and East Asia with strong correlations to summer precipitation in eastern China (Namias, 1959; Sud et al., 1988; Wang et al., 2009). Short-term climate prediction studies also indicate that snowfall anomalies in winter and spring over the TP can have trans-seasonal impacts on surface heat fluxes, influencing the intensity and onset of the Asian summer monsoon and causing summer precipitation anomalies across China (Li & Wang, 2020).

Given its persistent effect, SM can serve as a precursor signal for climate prediction (C. Zhu et al., 2023; X. Zhu et al., 2023). Several studies have highlighted the potential role of SM in subseasonal and seasonal forecasts (Douville et al., 2007; Grimm et al., 2007; Seneviratne et al., 2010). Current research has shown that positive spring SM in eastern TP reduces summer precipitation in south China and the Yellow River Basin but increases precipitation in the Yangtze River Basin and Northeast China (Yang & Wang, 2019). The possible mechanism is that summer atmospheric diabatic heating rate anomalies enhance the thermal forcing of the TP and the subtropical westerlies, thereby influencing the propagation of Rossby wave trains over midlatitudes. Another study identified a dipole variation between spring TPSM anomalies and summer precipitation in the Yangtze River Basin (C. Zhu et al., 2023; X. Zhu et al., 2023). They suggested that positive spring TPSM enhances diabatic heating during the summer, triggering upward motion over TP, accompanied by divergence in the upper troposphere and downward motion over the western Pacific. This promotes the intensification and northward movement of the South Asian High and the West Pacific Subtropical High. As a result, warm, moist air from the Bay of Bengal and the western Pacific converges with cold, dry air from the northern continent leading to excessive summer precipitation in the Yangtze River Basin. Meanwhile, (Yuan et al., 2021) found that surface SM in central and southern TP is positively correlated with summer precipitation in south China but negatively correlated with SM in the middle and lower reaches of the Yangtze River and Northeast China. The possible explanation is that when the surface SM in the central and southern TP is relatively high in May, surface heating is reduced, and as the thermal effect of TP weakens, upward motion decreases, causing the westerly jet to shift northward in the exit region of the East Asian Jet. This leads to a weaker western Pacific subtropical high and a more northward shift of the rain belt. Additionally, there is a correlation between TPSM and the climate in Northeast China on a seasonal scale (Han et al., 2024). A possible mechanism suggests that a stronger spring atmospheric heat source increases summer precipitation in Northeast China with SM in the Yellow River Basin and North China acting as a bridge. Owing to the "memory" effect of SM, this bridge can persist from spring to summer. The reduced land-ocean thermal contrast weakens the southward winds in the East Asia-West Pacific region as well as convection activity in the South China Sea and the tropical western Pacific. As a result, the East Asia-Pacific teleconnection pattern is modified leading to cyclonic anomalies and excessive summer precipitation over Northeast China.

The above research primarily explores the potential of TPSM as a precursor signal for seasonal-scale climate prediction with a focus on the East Asian monsoon region. However, studies on the impact of TPSM on precipitation in Northwest China (NWC) remain limited. The thermal effects of the TP significantly influence precipitation anomalies in NWC. When sensible heat is weak on TP in May and strong in the desert regions to its northwest, the position of the subtropical westerly jet in the West Asia shifts southward (Zhao et al., 2013). This results in anomalous cyclonic and anticyclonic circulation at 500 hPa over central Asia and Lake Baikal, respectively, causing southerly flow anomalies over northern Xinjiang province in China. This promotes the northward movement of warm and moist air from low latitudes, triggering precipitation. Another study suggested that spring snowmelt on TP significantly affects both spring and summer precipitation in NWC (Wang et al., 2023). The possible mechanism is that increased spring snowmelt on TP leads to higher SM, which, by altering the thermal forcing of TP, weakens the subtropical westerlies over Xinjiang. These anomalous

atmospheric conditions subsequently transport moisture into NWC, resulting in excessive summer precipitation in the region. How do TPSM and its thermal effects influence precipitation in NWC? What are the underlying physical mechanisms? Can TPSM serve as a precursor signal for summer precipitation in NWC? Exploring these key questions is crucial for improving our understanding of and predicting summer precipitation in NWC.

Since precipitation in NWC is primarily concentrated in the summer, this study will focus on the precursor signal of TPSM during spring investigating the physical processes through which TPSM influences summer precipitation in NWC. Sensitivity experiments using the Community Earth System Model 2 (CESM2) will also be conducted to validate the theoretical findings. The second section introduces the data and methods used; the third section explains the mechanisms by which SM in the northern TP affects precipitation in NWC; the fourth section presents model validation; the fifth section provides a summary and outlook.

2. Data and Methods

2.1. Data

2.1.1. Study Area

This study mainly focuses on the TP and NWC. The boundary of TP is derived from the Qinghai-Tibet Plateau of the National Basic Geographic Information Center of China (National Basic Geographic Information Center, 2019) and the boundary of northwestern China is provided by the National Cryosphere Desert Data Center (<http://www.ncdc.ac.cn>).

2.1.2. Reanalysis Data

This study primarily uses the Japanese 55-year Reanalysis (JRA55) data, which is produced using the Japan Meteorological Agency's (JMA) operational data assimilation system, TL319 version (Kobayashi et al., 2015). The observational data used in JRA55 cover global conventional radiosonde observations starting from 1958. The data used in this study mainly span from 1961 to 2020 and include three-dimensional wind, geopotential height, divergence, vertical heating rate profiles, SM, surface temperature, latent and sensible heat fluxes, relative vorticity, and potential vorticity, among others. The SM data primarily represent the surface SM (0–10 cm).

2.1.3. Precipitation Data

Precipitation data are selected from the gridded daily observation data set for China (CN05.1) based on observations from over 2,400 ground meteorological stations across China. The data set is constructed using a “climatology interpolation” method with a temporal resolution of 1 day and a spatial resolution of $0.25^\circ \times 0.25^\circ$ (Wu & Gao, 2013). In this study, the daily precipitation data for China from 1961 to 2020 are processed into monthly average precipitation data, and the precipitation amounts for June, July, and August of each year are used to represent summer precipitation in NWC for further analysis.

2.2. Methods

2.2.1. Statistical Methods

Singular value decomposition (SVD) and composite analysis are used in this study. Singular value decomposition is employed to examine the statistical relationship between surface TPSM during April and May (1961–2020) and precipitation in NWC. Composite Analysis is used to analyze the anomalies of circulation and the integrated water vapor flux corresponding to SM anomalies. Except for using North's Rule of Thumb (North et al., 1982) in the SVD analysis, the two-tail *t*-test was adopted in all other analyses.

2.2.2. T-N Wave Flux

This study uses wave flux to analyze the propagation of wave trains associated with mid-to upper-tropospheric atmospheric teleconnections (Takaya & Nakamura, 2001). This method is particularly suitable for studying the propagation paths and mechanisms of atmospheric teleconnection wave trains helping to understand the wave characteristics in large-scale atmospheric dynamics. The expression for its horizontal component is as follows:

$$W = \frac{P \cos \varphi}{2|\bar{U}|} \left\{ \begin{array}{l} \frac{\bar{u}}{a^2 \cos^2 \varphi} (\psi'_x - \psi' \psi'_{xy}) + \frac{\bar{v}}{a^2 \cos \varphi} (\psi'_x \psi'_y - \psi' \psi'_{xy}) \\ \frac{\bar{u}}{a^2 \cos \varphi} (\psi'_x \psi'_y - \psi' \psi'_{xy}) + \frac{\bar{v}}{a^2} (\psi'^2_y - \psi' \psi'_{yy}) \end{array} \right\} \quad (1)$$

where the overline and prime symbols represent the climate state and perturbation, respectively. $|\bar{U}|$ represents the wind speed, whereas \bar{u} and \bar{v} denote the zonal and meridional components of the wind, respectively. P , φ , a represent pressure, latitude, and the Earth's radius, respectively. $\Psi' = \frac{\psi'}{f}$, $f = 2\Omega \sin \varphi$, and ϕ and Ω are the potential and the earth rotation rate, respectively. The subscripts x and y indicate partial derivatives with respect to the zonal and meridional directions. By analyzing the magnitude and direction of the wave flux, the propagation characteristics of atmospheric waves, including the direction and intensity of wave energy transfer, can be quantitatively assessed.

2.2.3. CESM2 Numerical Model

The Earth system model CESM v2.2.0 (Danabasoglu et al., 2020), developed by the National Center for Atmospheric Research (NCAR), is used in this study. The Community Atmosphere Model (CAM) and the Community Land Model (CLM) are the main components utilized. CAM is a comprehensive atmospheric model that includes various processes such as radiation transfer, precipitation and cloud microphysics, cloud formation, boundary layer and surface flux exchange as well as momentum and energy dissipation. The version used is v6.0. CLM is a detailed land surface model that simulates a wide range of physical processes, including biogeophysical, hydrological, biogeochemical, and dynamic vegetation processes. These capabilities enable the model to simulate physical processes related to vegetation cover and soil heat-water transfer. The version used is v5.0, which incorporates improvements in key processes, including soil and vegetation hydrological processes, snowmelt dynamics, carbon and nitrogen cycles, coupled simulations, and vegetation modeling. Detailed specifications of the model are presented in Chapter 4.

3. Results

3.1. The Relationship Between TPSM and Precipitation in NWC

To investigate the impact of soil moisture (SM) on surface thermal conditions and atmospheric circulation, this study focuses on years with anomalously high and low SM in the spring and summer over the northern TP from 1961 to 2020. Specifically, years with SM anomalies exceeding ± 0.5 standard deviations are selected. The study aims to explore how these SM anomalies influence summer precipitation patterns in NWC. To minimize the impact of soil freeze-thaw processes on SM, March SM data are excluded. Instead, the 2-month average of surface SM for April-May is used to represent spring SM conditions over the TP, whereas the average of surface SM for June-August is used to represent summer SM.

The SM in the TP during spring and summer was de-trended to eliminate the influence of global warming and then analyzed by SVD with the summer precipitation in the NWC. The explained variance for the first mode of the SVD decomposition of spring (summer) TPSM and summer precipitation in NWC is 54% (75%), respectively (Figure 1). The significant regions of TPSM in both spring and summer are primarily located in northern TP (north of 32°N), whereas the significant precipitation areas in NWC are mainly concentrated in the southwestern and southeastern parts. The significant areas in the west and east exhibit a same variation with SM anomalies on TP. The correlation between the time series of TPSM and precipitation in NWC is 0.56 in spring and 0.64 in summer both passing the 99% significance test. This suggests that, statistically, there is a close relationship between spring SM over the northern TP and summer precipitation in NWC. As SM in northern TP increases or decreases, precipitation in the western and eastern parts of NWC also varies accordingly. This study will further investigate the connection and underlying physical processes between these two variables. In the following description, all the northern parts of the plateaus and their area average calculations are based on the region north of 33°N in the TP.

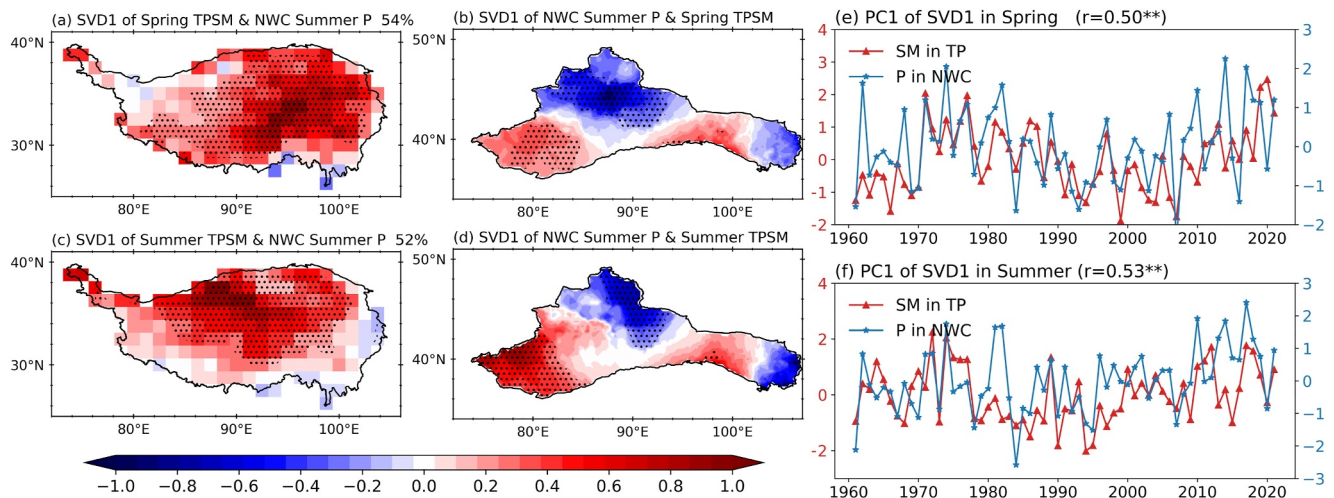


Figure 1. Decomposition of NWC Spring/Summer SM and singular value decomposition (SVD) of summer precipitation after de-trend. The first row presents the first mode of SVD decomposition for spring TPSM (a) and summer precipitation in NWC (b) along with the corresponding time series (e). The second row presents the first mode of SVD decomposition for summer TPSM (c) and summer precipitation in NWC (d) with the corresponding time series (f). The dotted areas indicate regions passing the 95% significance test. In the line plots, asterisks denote statistical significance at the 99% level.

3.2. Persistence of Spring SM Anomalies on TP

To investigate the relationship between spring and summer TPSM, Figure 2a shows the correlation of spring and summer TPSM from 1961 to 2020. The results indicate that significant regions are concentrated in northern TP suggesting strong persistence of SM in this region. Spring SM anomalies in the northern TP can persist into the summer (Li et al., 2016). The northern TP tends to be drier with SM often remaining at low levels, which promotes the persistence of anomalous conditions and results in a longer memory duration (Rahmati et al., 2024).

To further investigate how spring SM anomalies influence summer TPSM, high-pass filtering was applied to remove decadal variability with periods longer than 10 years from the spring and summer SM in northern TP retaining only the interannual variability. All the other variables in the following discussion have also undergone the same filtering processing to remove decadal variability. Scatter plots of spring and summer SM are shown in Figure 2b. The first (third) quadrant of the plot represents years in which both spring and summer SM in northern TP show positive (negative) anomalies. Years with persistent positive and negative SM anomalies were selected using 0.5 times the standard deviation as the threshold. Ten years with persistent positive anomalies were identified: 1964, 1972, 1977, 1981, 1989, 1996, 2002, 2005, 2012, and 2019, whereas eight years with persistent

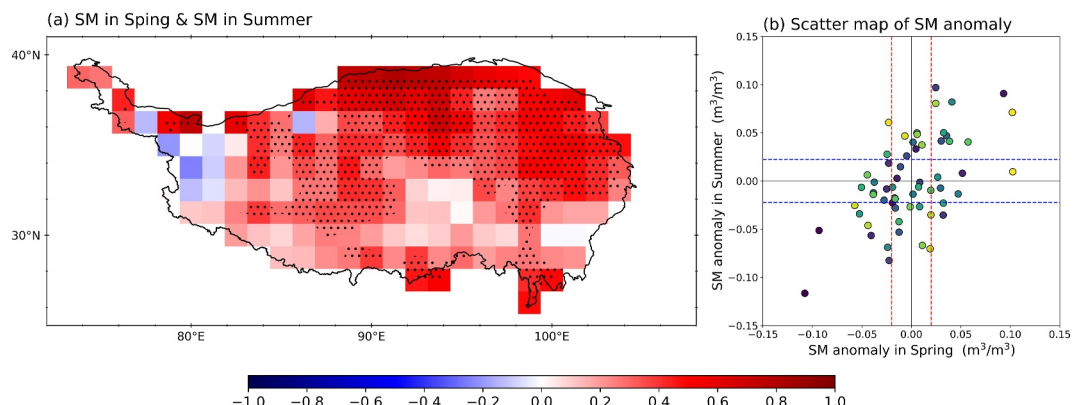


Figure 2. The correlation of spring and summer SM and the scatter plot of spring and summer SM anomaly. (a) Spatial distribution of the correlation coefficient between spring and summer SM with dotted areas indicating regions passing the 95% significance test. (b) Scatter plot of anomalies in spring surface SM (x-axis) and summer surface SM (y-axis) over the TP. The red and blue dashed lines represent 0.5 times the standard deviation of spring and summer SM, respectively.

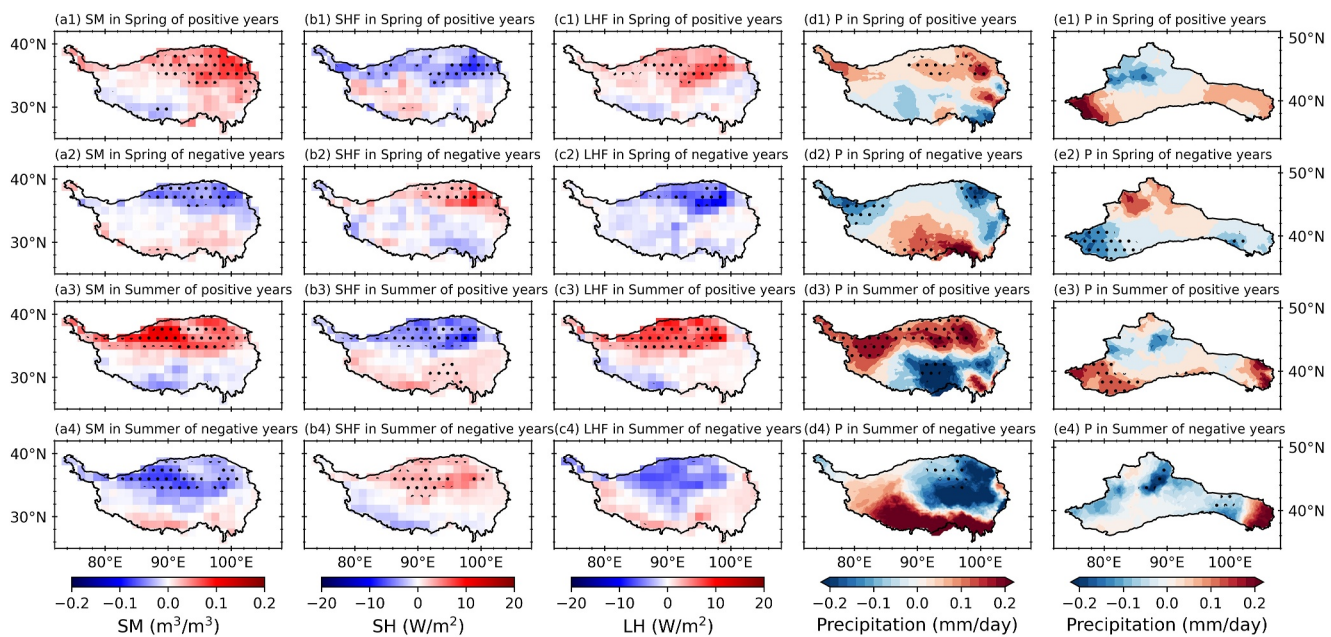


Figure 3. Anomalies of surface flux and precipitation (P) from positive and negative abnormal years of SM. Panels (a1–e1) show the SM, SHF, LHF, and P for years with positive SM anomalies in spring, respectively. Panels (a2–e2) are the same as panels (a1–e1) but for negative SM anomalies. Panels (a3–e3) and (a4–e4) are the same as panels (a1–e1) and (a2–e2) but for summer. Dotted areas in the figures indicate regions where the results pass the 90% significance test.

negative anomalies were identified: 1961, 1962, 1968, 1973, 1990, 1994, 2014, and 2016. The persistence of spring and summer SM anomalies is then examined by analyzing the differences in the annual average SM values for these years relative to the climatology. Unless otherwise noted, the analyses in this paper are based on positive/negative SM anomalies in northern TP, and the TPSM below refers to SM in the northern TP.

How spring TPSM persists into summer is discussed below. Figure 3 shows the changes in surface SM, surface sensible heat flux (SHF), and surface latent heat flux (LHF) for years with positive/negative SM anomalies. It is observed that positive or negative spring TPSM (Figures 3a1 and 3a2) correspond to a rise or fall in evapotranspiration (ET), a negative or positive SHF (Figures 3b1 and 3b2), and a corresponding change in surface LHF (Figures 3c1 and 3c2). Additionally, spring precipitation in the northern TP exhibits positive/negative anomalies (Figures 3d1 and 3d2) subsequently affecting SM levels. Previous studies have shown that precipitation accounts for more than 80% of the relative contribution to SM changes in TP (Bai et al., 2019). Figures 4a and 4b show the average sensible heat flux (SH), latent heat flux on the ground (LH), SM (mm^3/mm^3) and precipitation (mm/day) of each month from March to August in the northern TP with positive anomaly years minus negative anomaly years. Increased spring SM over the northern TP enhances surface evapotranspiration, which amplifies LH release and increases precipitation through moisture recycling (Figure 4a). The resultant precipitation surplus effectively replenishes SM depletion induced by intensified ET establishing a self-sustaining coupling mechanism between precipitation and SM. This feedback process persists from March to July (Figure 4b) maintaining the positive SM anomalies from spring to summer (Yang et al., 2016).

The SM can persist for several days or even months, thereby influencing subsequent thermal and circulation changes through land-atmosphere interactions (Grimm et al., 2007; Quesada et al., 2012; Zhang & Zuo, 2011). In spring, the surface temperature on TP remains relatively low and the unique freeze-thaw characteristics allow the SM anomaly to persist for more than 3 months (Wang et al., 2020). Moreover, SM anomalies can also influence atmospheric circulation anomalies, which, in turn, affect precipitation. According to thermal adaptation relationships, circulation anomalies caused by latent heat (LH) release from precipitation condensation lead to enhanced southerly winds over TP, increased summer monsoon precipitation, and a stronger northward shift of the TP monsoon (Zhou et al., 2018). This results in a positive transport of moisture from the southern to the northern TP with concurrent upward motion in northern TP, leading to positive summer precipitation (Figure 3d3), positive SM (Figure 3a3), negative SHF (Figure 3b3), and positive LHF (Figure 3c3). These processes help sustain the SM anomalies in the northern TP from April-May through August.

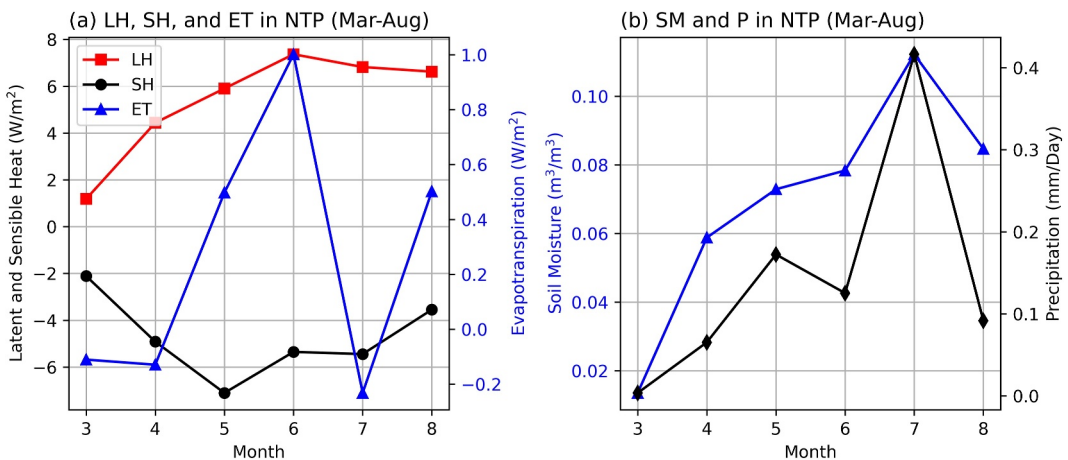


Figure 4. The monthly changes of sensible heat (black line in subfigure a), latent heat (red line in subfigure a), surface evapotranspiration (ET) (blue line in subfigure a), SM (blue line in subfigure b), and precipitation rate (black line in subfigure b) in SM positive anomaly years minus negative anomaly years.

3.3. The Physical Mechanism

Anomalous summer TPSM, along with anomalous precipitation, influences the atmospheric heat source over northern TP, which in turn induces circulation anomalies that affect surrounding regions. Figures 3e3 and 3e4 show the spatial distribution of NWC summer precipitation corresponding to the years with positive and negative SM anomalies. The results show that positive (negative) TPSM anomaly is associated with corresponding positive (negative) precipitation anomaly in the western and eastern parts of NWC during both spring and summer. To clarify the impact of anomalies of TPSM on precipitation in NWC, the atmospheric heating anomalies associated with the TP, caused by anomalies of TPSM, are analyzed first.

Generally, TPSM influences the atmospheric heat source, which subsequently affects the atmospheric circulation in the surrounding and downstream regions (Luo et al., 2024). The atmospheric heating rate in northern TP is partitioned into four components: sensible heating rate (SHR), latent heating rate (LHR) of condensation, shortwave radiation heating rate (SWHR), and long-wave radiation heating rate (LWHR). The difference between positive and negative SM anomaly years for each component reveals that when positive TPSM anomaly occurs during summer, both SHR and LWHR decrease (Figures 5a and 5c), whereas LHR and SWHR increase (Figures 5b and 5d) resulting in an overall increase in the atmospheric heating rate (Figure 5e). In other words, a positive TPSM anomaly leads to a reduction in surface temperature, which is induced by negative SHR at the surface and positive LHR. Consequently, positive TPSM increased precipitation and cloud cover. The LHR released by precipitation warms the atmosphere, causing an increase in atmospheric temperature, enhanced long-wave radiation cooling and a positive SWHR due to absorbed solar radiation by the increased water vapor. The combined effects of these heating and cooling processes result in an overall positive atmospheric heat source.

By analyzing the vertical profiles of each heating rate (Figure 5f), it is found that the LHR of condensation in the northern TP first increases and then decreases as it rises from the surface. The peak heating center occurs around 400 hPa where LHR dominates the atmospheric total heating rate (THR). SHR remains relatively uniform from the surface to 500 hPa but then rapidly decreases reaching zero at around 400 hPa. SWHR shows minimal variation during positive and negative SM anomalies. The influence of TPSM on LWHR in the atmosphere is not statistically significant from the surface to 500 hPa. During positive TPSM anomalies, LWHR above 500 hPa has a cooling effect on the atmosphere due to increased cloud cover in the atmosphere, which enhances LWHR emitted from the cloud layer (Lin et al., 2023).

Subsequently, the circulation anomalies induced by thermal source anomalies over northern TP are discussed. Figures 6a–6e show the geopotential height with the zonal mean removed at 550, 400, and 200 hPa as well as the integrated moisture flux divergence fields composited by positive and negative SM anomaly years. The results indicate that when there is a positive TPSM anomaly during summer, a negative geopotential height anomaly extends from 550 to 200 hPa in the western part of NWC, whereas a positive geopotential height anomaly is

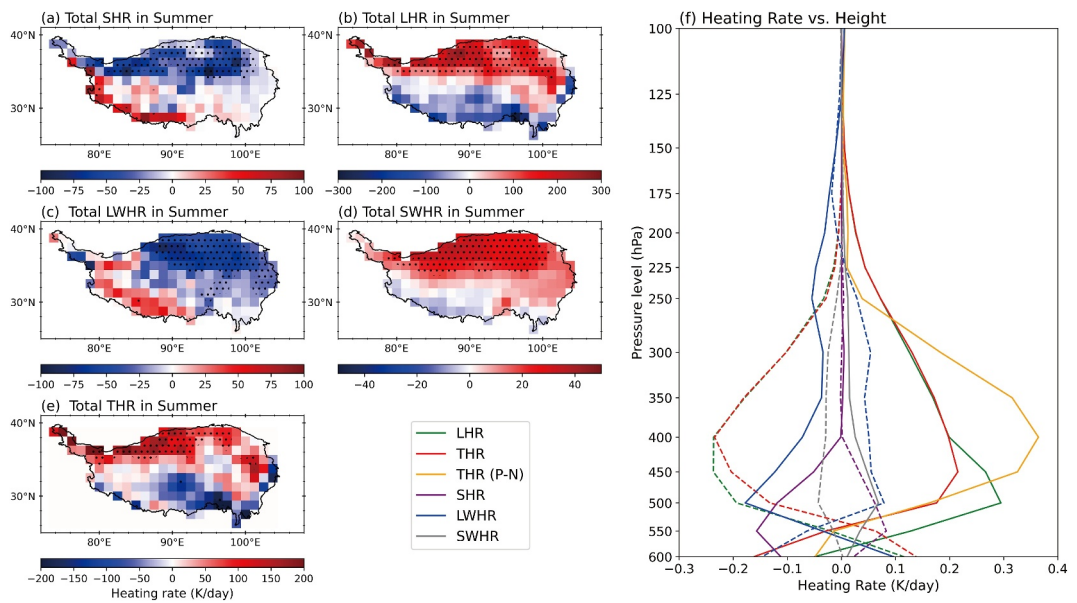


Figure 5. Composite differences between the positive and negative SM anomaly years over the Tibetan Plateau (TP) for (a) sensible heat rate (SHR), (b) latent heat rate of condensation (LHR), (c) longwave cooling rate (LWHR), (d) solar shortwave heating rate (SWHR), and (e) total heating rate (THR). Dotted areas represent regions passing the 90% significance test. On the right, the vertical profiles of the average SHR (purple), LHR (green), LWHR (blue), SWHR (gray), and THR (red) over the northern TP are shown. The orange line represents the difference of THR between the positive and negative SM anomaly years with solid lines indicating the average for positive anomaly years and dashed lines indicating the average for negative anomaly years.

observed in the eastern part. With increasing altitude, the anomalies in geopotential height become more pronounced. The anomalous geopotential height induces a cyclonic circulation anomaly that develops in the western part of NWC leading to a southerly wind anomaly in this region. In the eastern part of NWC, an anticyclonic circulation anomaly is presented resulting in an easterly wind anomaly in this area. At 550 hPa, a negative geopotential height anomaly is observed in northern TP, and as the altitude increases, the center of the anomaly shifts westward. At 200 hPa, the anomalous cyclonic circulation center is located over western TP.

The mechanism by which thermal source anomalies in northern TP lead to the aforementioned circulation anomalies is examined by analyzing the full vertical vorticity equation as written by Liu et al. (1999):

$$\frac{\partial \zeta}{\partial t} + V \cdot \nabla \zeta + \beta \nu = -(f + \zeta) \nabla \cdot V + \frac{1}{\alpha} \frac{d}{dt} \left[\frac{P_E}{\theta_z} - C_D \right] + \frac{1}{\theta_z} F_\zeta \cdot \nabla \theta_z + \frac{f + \zeta}{\theta_z} \frac{\partial Q}{\partial z} - \frac{1}{\theta_z} \frac{\partial v}{\partial z} \frac{\partial Q}{\partial x} + \frac{1}{\theta_z} \frac{\partial u}{\partial z} \frac{\partial Q}{\partial y}, \theta_z \neq 0 \quad (2)$$

where $Q = Q_{LH} + Q_{SH} + Q_{LWH} + Q_{SWH}$, representing LHR, SHR, LWHR, and SWHR, respectively. The first four terms on the right side represent divergence of vorticity, changes in the internal thermal structure, and the effects of frictional dissipation on vorticity changes with the last three terms representing contributions from spatially inhomogeneous heating. Under the assumptions of no changes in the internal atmospheric structure, no friction, and consideration of only diabatic heating, Equation 2 becomes

$$\frac{\partial \zeta}{\partial t} + \frac{V \cdot \nabla \zeta}{L_2} + \frac{\beta \nu}{L_3} = \frac{-(f + \zeta) \nabla \cdot V}{R_1} + \frac{\frac{f + \zeta}{\theta_z} \frac{\partial Q}{\partial z}}{R_2} - \frac{\frac{1}{\theta_z} \frac{\partial v}{\partial z} \frac{\partial Q}{\partial x}}{R_3} + \frac{\frac{1}{\theta_z} \frac{\partial u}{\partial z} \frac{\partial Q}{\partial y}}{R_4} \quad (3)$$

where β is the Rossby parameter, k is the specific volume, f is the Coriolis parameter, θ_z represents the vertical gradient of potential temperature and ξ is vorticity with the other symbols denoting commonly used meteorological variables.

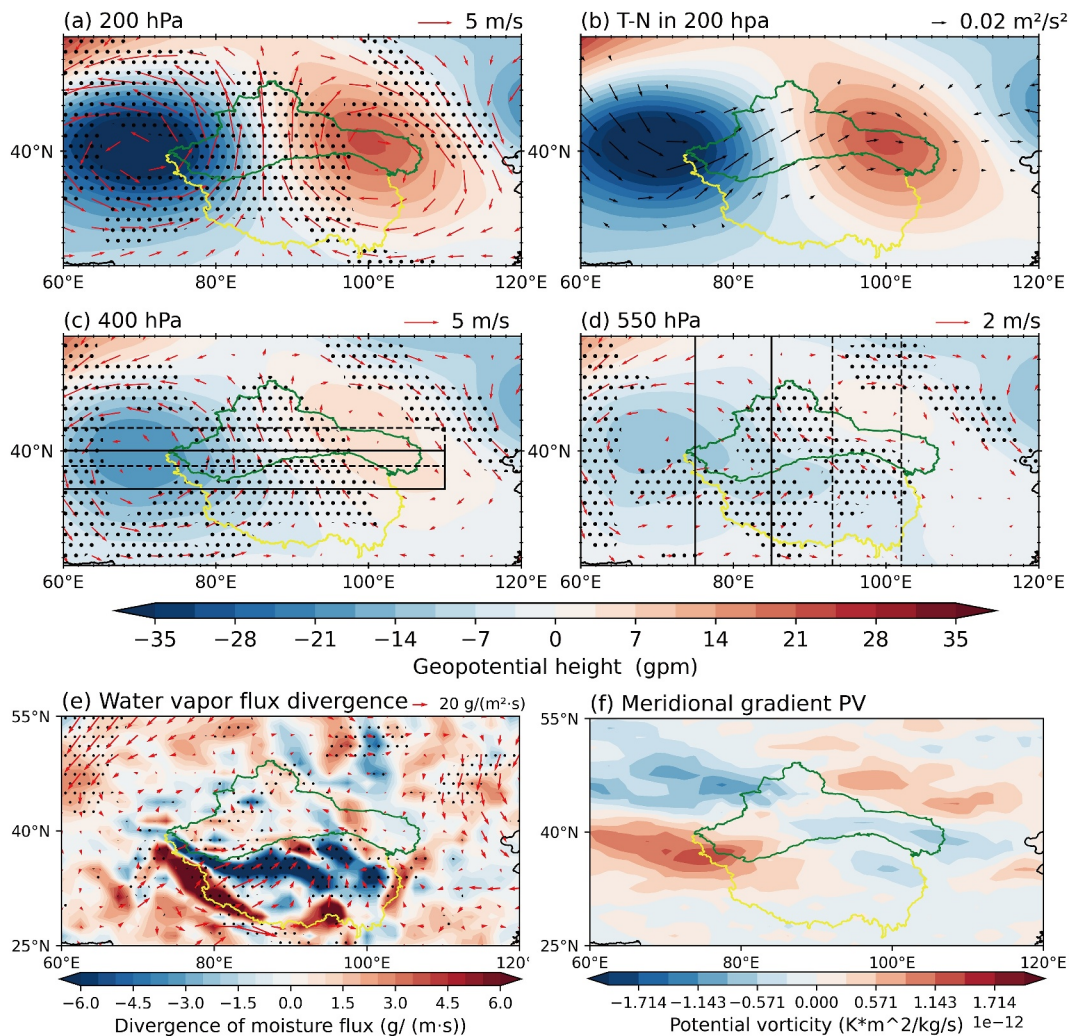


Figure 6. The composite differences in geopotential height anomalies (with the zonal mean removed) during summer at 200 hPa (a), 400 hPa (c), and 550 hPa (d) were obtained by subtracting the circulation fields with negative SM anomaly years from those with positive SM anomaly years. The corresponding T-N flux at 200 hPa of the composite difference is shown by the black arrow in panel (b). Red arrows indicate wind speed, and the shaded areas represent geopotential height anomalies. The boundaries of TP and NWC are outlined by yellow and green lines, respectively. (e) Integrated moisture flux (vectors) and moisture flux divergence (shading) for the difference between positive and negative SM anomaly years. (f) Meridional gradient of the potential vorticity on the 370 K isentropic surface (about 200 hPa) for the difference between positive and negative SM anomaly years. The dotted areas in the figures indicate regions passing the 95% significance test. In Figure 6c, the black solid and dashed rectangles represent the profile ranges shown in Figures 8c and 8d, respectively. In Figure 6d, the black solid and dashed rectangles represent the profile ranges shown in Figures 8a and 8b.

Through the scale analysis, for long-term variations, local changes in vorticity can be estimated, and in the lower levels of the subtropics where the zonal winds are weak ($u \approx 0$), advection is negligible. Based on the calculations of the positive and negative anomalies in Equation 3, at 500 hPa, L₁ and L₂ are on the order of 10^{-15} , R₁ is on the order of 10^{-13} , R₂ and R₄ are on the order of 10^{-11} , and R₃ is approximately 10^{-12} . The key contributions to vorticity in Equation 3 are shown in Figures 7a–7c. The results indicate that below 400 hPa, the vertical heating gradient plays a dominant role in vorticity changes with vorticity variations induced by vertical motion being smaller in magnitude than those driven by vertical changes in the heat source. Furthermore, the changes in the meridional wind component due to the β -effect are mainly balanced by the vertical heating term.

Therefore, below the center of maximum heating, Equation 3 can be simplified as

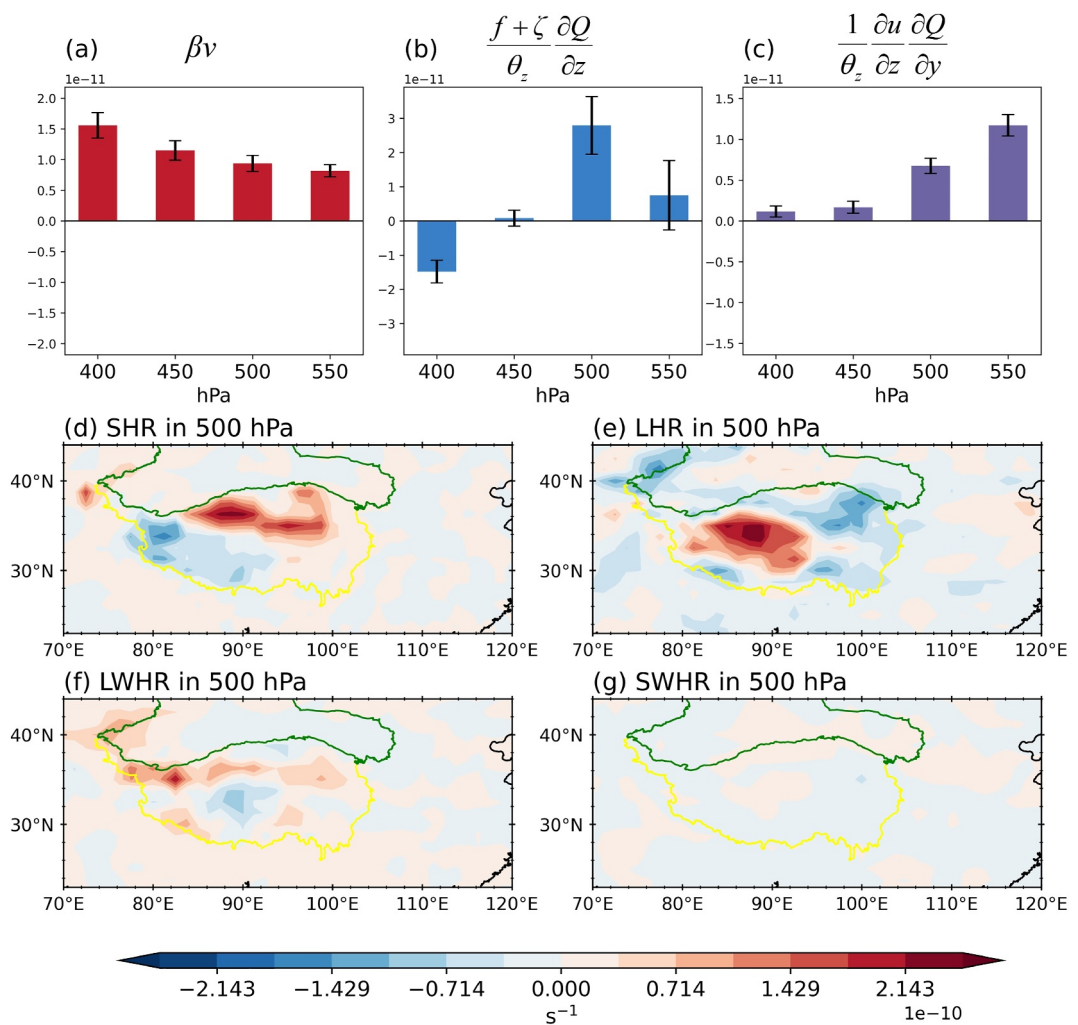


Figure 7. The calculation results of each item in Equation 3. (a–c) Averaged values of the main contributing terms in Equation 3 for the difference between positive and negative SM anomaly years at 400, 450, 500, and 550 hPa over northern TP. The second and third rows show the decomposition of the vertical thermal gradient terms for difference between positive and negative SM anomaly years at 500 hPa: (d) SHR, (e) LHR, (f) LWHR, and (g) SWHR.

$$\beta\nu \propto \frac{f + \zeta}{\theta_z} \frac{\partial Q}{\partial z} \quad (4)$$

Under the β -effect, southerly winds develop beneath the thermal source center, inducing a cyclonic circulation anomaly to the west of the heat source (Figure 6a). To further clarify the contribution of each heating term, Q in Equation 4 is decomposed into Q_{LH} , Q_{SH} , Q_{LWH} and Q_{SWH} . Figures 7d–7g illustrate the decomposition of the right side of Equation 4 at 500 hPa for the four heating terms obtained as the difference between positive anomalies and negative anomalies. The results show that, at 500 hPa, the primary contribution to the right-hand side of Equation 4 comes from the vertical gradients of SHR, LHR, and LWHR, and their vertical gradients are also much smaller than that of LHR. However, as indicated by the analysis in Figure 5, the magnitudes of SHR and LWHR are significantly smaller than that of LHR, and their vertical gradients are also much smaller than that of LHR. Therefore, this study primarily focuses on the thermal anomalies caused by latent heat of condensation. When a positive anomaly in LHR occurs in northern TP, the significant release of latent heat alters the vertical temperature gradient over the region. The anomalous LHR generates a southerly wind anomaly in northern TP (Figures 6c and 6d) (Liu et al., 1999), which, in turn, drives a cyclonic circulation anomaly over the western TP. In the upper atmosphere over the midlatitudes, the atmospheric

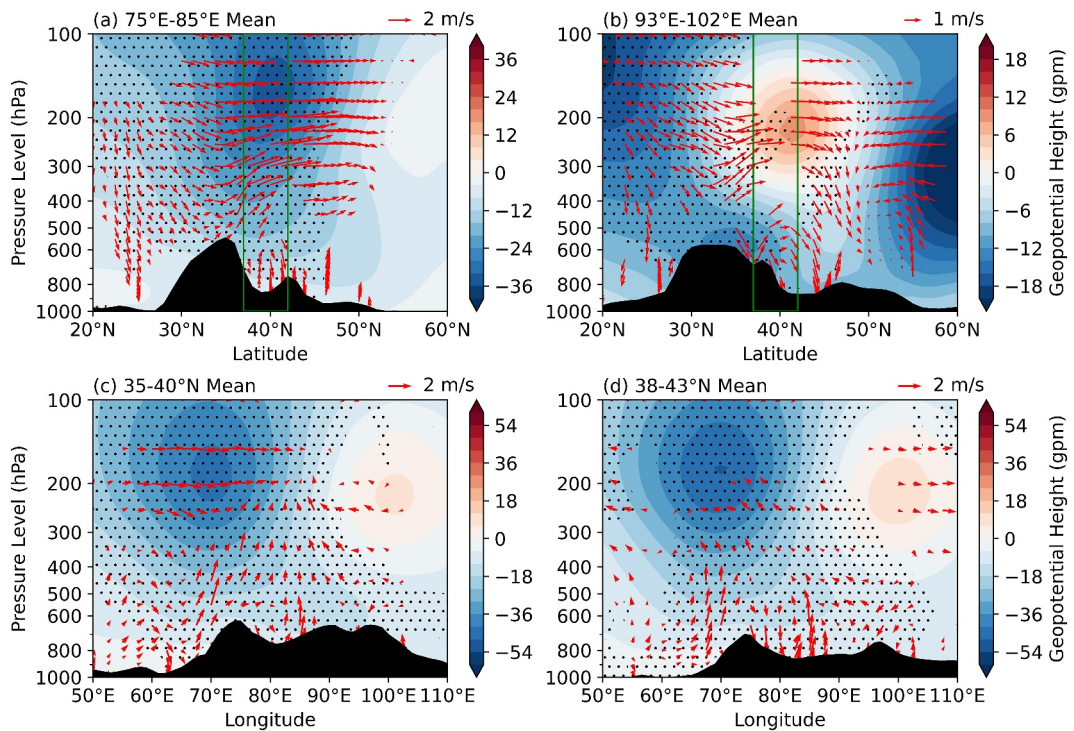


Figure 8. The difference between positive and negative SM anomaly years for averaged vertical circulation in summer at (a) 75°N – 85°N , (b) 93°E – 102°E , (c) 35°N – 40°N , and (d) 38°N – 43°N . The black shading represents topography, and the black dotted areas indicate regions passing the 90% significance test. The background shading represents the difference of geopotential height between positive and negative SM anomaly years with units in gpm. The vertical velocity is amplified by a factor of 100 for emphasis. The green lines in panels (a, b) represent the southern boundary of NWC arid region spanning 37°N to 42°N .

response to transient vorticity forcing dominates, and the circulation anomaly manifests as a quasi-barotropic structure in the mid-to-high latitudes (Fang & Yang, 2016).

This study suggests that a positive SM anomaly in northern TP induces a southerly wind anomaly, which, in turn, generates a cyclonic circulation anomaly on the western side of TP. This circulation anomaly influences both precipitation and SM in northern TP further reinforcing the cyclonic circulation and contributing to increased summer precipitation in NWC. Regarding the anticyclonic circulation anomaly in the northern NWC, positive precipitation in northern TP induces positive LHR, leading to a positive vorticity anomaly on the 370 K isentropic surface, corresponding to approximately 200 hPa (Figure 6f). This enhances the meridional gradient of vorticity between the TP and NWC guiding wave trains toward NWC. Additionally, the T-N wave flux at 200 hPa , obtained by subtracting negative anomalies from positive anomalies (Figure 6b), shows that the cyclonic vorticity anomaly on the western side of TP, induced by thermal adaptation, propagates northeastward through Rossby waves. This leads to the formation of a weak anticyclonic circulation anomaly in the northeastern part of NWC affecting the northern NWC.

To visually illustrate the vertical motion induced by the circulation anomalies in NWC, the latitudinal cross section within the black rectangle of Figure 6d is shown in Figure 8. The meridional vertical cross section from 93°E to 102°E (Figure 8b) reveals that the northern part of NWC, influenced by the anticyclonic circulation, experiences dominant subsiding motion, which leads to reduced precipitation in the northern arid regions. At 550 hPa , anomalous easterly winds are observed, bringing moisture into the eastern part of NWC (Figure 8e), resulting in increased precipitation in the southern NWC. In the western part of NWC, a deep low-pressure system extends from 550 to 200 hPa situated to the east of the cyclonic circulation center accompanied by a strong southerly wind anomaly and significant upward motion (Figure 8a). The positive-minus-negative anomaly analysis of the integrated moisture flux divergence indicate significant moisture convergence in the western arid

regions. The circulation and moisture flux fields are well-coordinated leading to positive precipitation anomaly in the western part of NWC.

4. Numerical Experiments

To validate the above theory, idealized simulations were conducted using the CESM2. The study employed two components of the model (Table 1) conducting experiments with anomalous atmospheric heating rate and anomalous TPSM.

4.1. Atmospheric Heating Rate Sensitivity Experiment

In the atmospheric heating rate sensitivity experiment, the FHS94 component was used with a simulation duration of 1,200 days. This component represents an idealized setup, considering only topography and dry atmospheric processes, without external forcing such as solar angle or ocean effects. The first 200 days were designated as the model's equilibrium period, and the results were analyzed by averaging the final 1,000 days. Three atmospheric heating rate sensitivity experiments were conducted over northern TP (Figure 9b2): Experiment 1, the THR anomaly experiment, incorporates the heating rate represented by the orange line in Figure 7f; Experiment 2, the LHR anomaly experiment, includes the difference between the solid and dashed red lines; Experiment 3, the SHR anomaly experiment, incorporates the difference between the solid and dashed purple lines.

As shown in Figure 9, by comparing the sensitivity experiments of the three kinds of heating rate anomalies, it is found that the circulation anomalies caused by the heating anomaly of latent heat of condensation are highly consistent with that of the THR. In contrast, SHR anomalies produce the opposite effect of LHR but with a weaker intensity. This suggests that when there is a positive SM anomaly in northern TP, LHR plays a dominant role in driving circulation anomalies, whereas SHR acts to weaken the circulation anomalies caused by LHR.

The results show that when a positive atmospheric heating anomaly occurs over northern TP, a negative geopotential height anomaly is induced at the surface over the northern TP (Figure 9a3). As altitude increases, the center of the negative geopotential height anomaly shifts westward, whereas the center of the positive geopotential height anomaly in the south shifts northward. Eventually, a cyclonic circulation anomaly develops to the west of the heating center with an anticyclonic circulation anomaly forming to the east (Figures 9a1 and 9b1). This circulation anomaly pattern is consistent with the cyclonic circulation anomaly in the western part of NWC and the anticyclonic anomaly in the eastern part of NWC shown in Figure 5 although with slight positional differences. This suggests that under the influence of atmospheric heating alone, a positive SM anomaly in the northern TP leads to a positive LHR. Through the thermal adaptation principle discussed in Section 3.3, this induces a cyclonic circulation anomaly to the west and an anticyclonic anomaly to the east of the heating center.

Since this component is an idealized experiment and does not consider moist processes or other weather phenomena, it cannot fully represent the role of TPSM. Therefore, a more complex sensitivity experiment with SM anomalies was conducted below.

4.2. SM Sensitivity Experiment

In the SM sensitivity experiment, this study used the F2000climo component conducted over northern TP (Figure 9b2). This component couples the atmospheric module with the land surface module specifically the coupling of CLM5 and CAM6. A positive SM anomaly was introduced to northern TP during spring and summer (April, May, June, July, and August) based on the positive-minus-negative anomalies shown in Figures 3a1, 3b1, 3c1, and 3d1. The SM anomaly was added as a monthly mean, rather than seasonal, to simulate the circulation anomalies induced by TPSM anomalies. The model was run for 30 years with the first 10 years serving as the equilibrium period, and the subsequent 20 years averaged for analysis. The average of June, July, and August was taken as the summer result for analysis.

The model simulation results show that in the absence of upstream wave train influences, when there is a positive SM anomaly in spring and summer over northern TP, a negative geopotential height anomaly is generated at 550 hPa (near the surface of TP) in summer (Figure 10d). As altitude increases, the center of the negative geopotential height anomaly gradually shifts westward. At 200 hPa, a band-like cyclonic circulation anomaly appears over western TP (Figure 10a) accompanied by an anticyclonic circulation anomaly in the northern part of NWC showing a quasi-barotropic structure (Figure 10b). This circulation anomaly configuration is consistent

Table 1
Two Components are Used By Models

Component	Scientifically grids	Details	Value	Description
F2000climo	f09_f09_mg17	Initialization Time	2,000	1850: Pre-Industrial; 2000 present day Additional initialization times defined by components
		Atmosphere	CAM60	CAM6 physics
		Land	CLM50%SP	clm5.0:Satellite phenology
		Sea-Ice	CICE%PRES	CICE (cice) model version 5;prescribed ice
		Ocean	DOCN%DOM	DOCN prescribed ocean mode
		River runoff	MOSART	MOSART: Model for Scale Adaptive River Transport
		Land Ice	CISM2%NOE-VOLVE	cism2 (default, higher-order, can run in parallel)cism ice evolution turned off (this is the standard configuration unless you're explicitly interested in ice evolution)
		Wave	SWAV	Stub wave component
FHS94	T42z30_T42_mg17	Initialization Time	2,000	1850: Pre-Industrial; 2000 present day Additional initialization times are defined by components
		Atmosphere	CAM%HS94	CAM simplified and nonversioned physics: CAM dry Held-Suarez forcing (Held and Suarez (1994))
		Land	SLND	Stub land component
		Sea-Ice	SICE	Stub ice component
		Ocean	SOCN	Stub ocn component
		River runoff	SROF	Stub river component
		Land Ice	SGLC	Stub glacier (land ice) component
		Wave	SWAV	Stub wave component

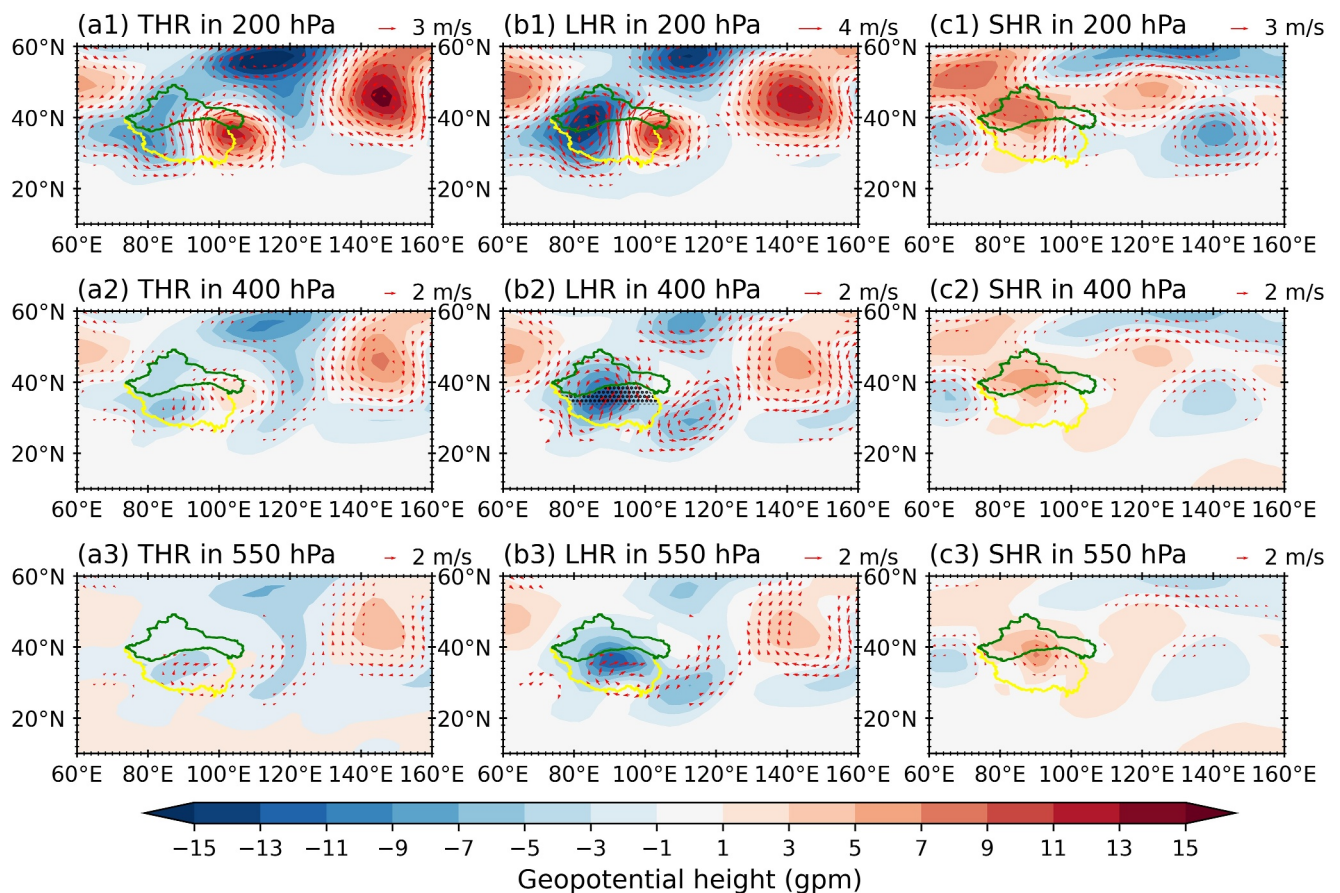


Figure 9. The results of the FHS94 experiment with heating rate anomalies comparing the difference between the control run and the sensitivity run. The anomaly profiles for total heating rate (positive anomalies minus negative anomalies) are shown for the 200, 400, and 550 hPa circulation fields in (a1, a2, a3). The circulation fields corresponding to the 200, 400, and 550 hPa levels are shown after adding only the latent heating rate anomaly profiles in (b1, b2, b3). The circulation fields for the 200, 400, and 550 hPa levels after adding only the SHR anomaly profiles are shown in (c1, c2, c3). In Figure 9b2, the black shaded area represents the region where the heating rate was modified in the sensitivity experiment.

with the results from the composite analysis (Figure 5a). At the same time, the 200 hPa T-N wave flux from the model simulation shows that the cyclonic circulation anomaly over western TP propagates northeastward via wave flux (Figure 10b), which is also consistent with the composite analysis results (Figure 5b). This suggests that when there is a SM anomaly in the northern TP, it leads to an anomaly in the vertical atmospheric heating profile primarily driven by LHR. Through the thermal adaptation principle, a cyclonic circulation anomaly is generated over the western TP, and this anomaly propagates eastward due to Rossby wave transmission inducing an anticyclonic circulation anomaly in NWC.

Generally speaking, SM and the atmosphere are highly coupled as discussed in Section 3.1. The SM in northern TP varies consistently with precipitation, and positive SM leads to positive precipitation, which in turn alters the thermal state of TP. However, in the model simulations, the SM forcing applied in this study is kept constant. The SM is interpolated into the model's time steps, meaning that a fixed value is assigned to SM. As a result, SM and atmospheric processes are partially decoupled in the model leading to persistently high SM throughout the simulation. Nevertheless, the SM forcing on the atmosphere as well as the energy exchange between the soil and the atmosphere remains persistent. Due to the more sustained SM forcing in the simulation, the negative vorticity anomaly at 550 hPa is quite strong covering the entire northern TP (Figure 10d). This could explain why the simulated results align with the observed anomalous circulation pattern albeit with minor differences in the location of the anomaly center.

Finally, the model's simulation of summer precipitation over the TP and NWC was conducted in this study (Figures 10e and 10f). The results show that when there is a positive SM anomaly in northern TP during spring

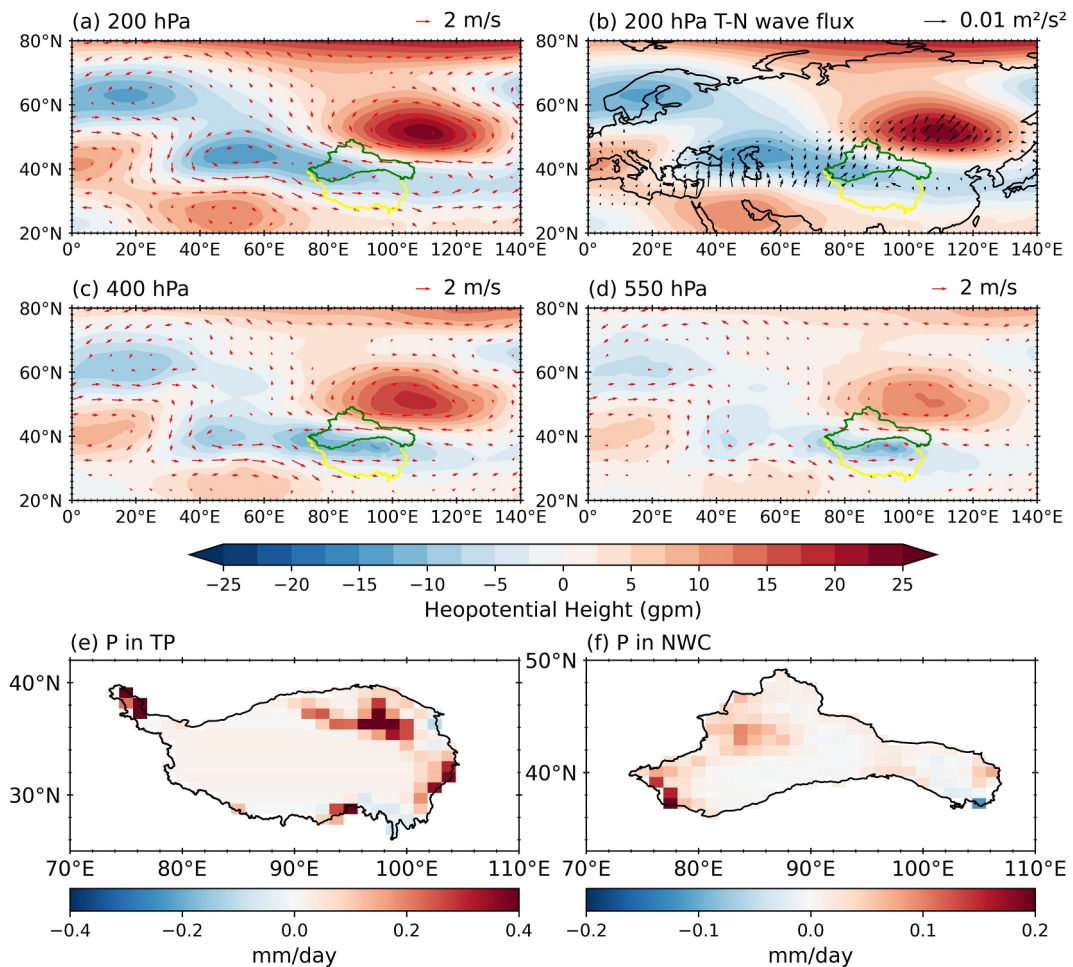


Figure 10. The results of SM anomalies from the F2000climo experiment (regions as in Figure 9b2), with the difference between the control run and the experimental run corresponding to the 200, 400, and 550 hPa circulation fields (a, c, d) and the T-N wave flux at 200 hPa (b). The background shading represents geopotential height with units in gpm. The third row shows the precipitation anomalies for summer in the northern TP (e) and NWC (f) after subtracting the control experiment from the experimental run.

and summer, the model simulates a positive precipitation anomaly in summer over northern TP, which is consistent with the composite analysis results (Figure 3d3). However, there are some differences in the results for NWC. The model shows an overall increase in precipitation over NWC, which slightly deviates from the observed pattern (Figure 3e3). This discrepancy may be attributed to the more persistent high SM forcing applied in the experiment.

5. Summary and Discussion

This study explored the impact of spring and summer SM in northern TP on precipitation in NWC from a statistical perspective using reanalysis data and further investigated the potential physical connections between them. Additionally, the CESM2 model was used to simulate the influence of TP spring and summer SM on summer precipitation in NWC and to explore the associated physical mechanisms (Figure 11).

The main conclusions of the study are as follows: the summer SM anomalies in northern TP are influenced by two main factors: first, when a positive SM anomaly occurs in spring over northern TP, it leads to increased evaporation, which generates more precipitation, thereby reinforcing the positive SM anomaly. As a result, the spring SM anomaly persists into summer through its positive feedback with precipitation. Second, the positive SM anomaly in northern TP induces a southerly wind anomaly through thermal adaptation, which in turn triggers a cyclonic circulation anomaly on the western side of TP. This strengthens the TP monsoon, leading to positive

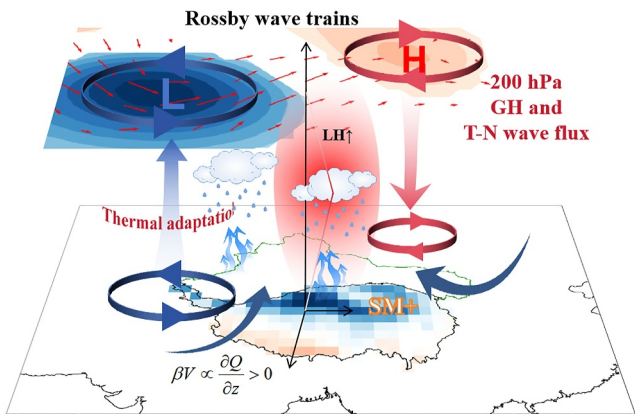


Figure 11. Schematic diagram illustrating the impact of TPSM anomalies on summer precipitation in NWC.

Similarly, simulations using the F2000climo model show that when there is a positive SM anomaly in northern TP, a cyclonic circulation anomaly forms in the western NWC, and an anticyclonic circulation anomaly generates in the eastern NWC. This is consistent with the results from the composite analysis. These results support the potential of using spring SM anomalies in northern TP as a precursor signal for summer precipitation prediction in NWC.

This study focuses solely on the thermal effects of TPSM on the increased summer precipitation in NWC, whereas the roles of other key regions are equally important. In the western Eurasian continent, there is a strong correlation between SM and summer precipitation in NWC. However, understanding the synergistic effects of upstream teleconnected wave trains, and to differentiate the impact of precursor signals of soil moisture in the northern plateau from the changes in northern plateau soil moisture induced by teleconnected wave trains as well as their effects on circulation, remains an area for further research. Additionally, the causes of precipitation in NWC are multifaceted. Previous studies have shown that the North Atlantic Oscillation (NAO) and upstream teleconnections play significant roles in modulating precipitation in NWC (Zhang et al., 2019; Zhou & Huang, 2010). One study highlighted the important modulating effect of Arctic sea ice on precipitation in NWC (Liu & Sun, 2024). Positive sea ice concentration anomalies in early autumn are linked to anomalous northeast winds, which lead to drier soils and widespread cooling over the East European Plain. This dry soil signal may persist until the following spring and early summer, triggering an anticyclonic circulation anomaly over Siberia, enhancing moisture convergence in NWC, and increasing humidity in the region. The findings of this study represent only a small part of a complex system. Further exploration is needed to investigate the synergistic effects between multiple complex systems such as Arctic sea ice, El Niño-Southern Oscillation, North Atlantic oscillation, and Silk Road Teleconnection.

This study primarily focuses on the relationship between interannual variability of TPSM and summer precipitation in NWC over the past 60 years. In the context of global warming, the response of TPSM and its contribution and mechanisms in the warming and moistening of NWC (Chen et al., 2023; Ding et al., 2023) still require further analysis. At the same time, whether the land-atmosphere interactions in NWC will amplify or mitigate the impacts from other regions remains to be investigated. Additionally, the synergistic effect between the SM of TP and that of NWC still requires further investigation. The use of TPSM for climate prediction in NWC will be a key focus of future research.

Conflict of Interest

The authors declare no conflicts of interest relevant to this study.

Data Availability Statement

The JRA55 reanalysis data (Kobayashi et al., 2015) are available at Japan Meteorological Agency/Japan (2013). The observational precipitation data were used from CN05.1 (Wu & Gao, 2013), which is available from this site

precipitation in northern TP and sustaining the SM anomaly until August. Additionally, the cyclonic circulation anomaly, through the propagation of Rossby waves, induced an anticyclonic circulation anomaly in the northern part of NWC. As a result, the western part of NWC is mainly controlled by the anomalous cyclonic circulation, characterized by anomalous upward motion and moisture convergence, leading to increased precipitation. In contrast, the northern part of NWC experiences an anticyclonic circulation anomaly causing subsidence and resulting in reduced precipitation. However, the easterly wind anomaly induced by the anticyclonic circulation enhances moisture transport resulting in increased precipitation in the southeastern part of NWC. This combination leads to the observed phenomenon: during spring, when there is a positive SM anomaly in northern TP, summer precipitation increases in the western part of NWC and decreases in the northern part.

The results of simulations using the FHS94 model show that anomalous heating rates in northern TP lead to a cyclonic circulation anomaly in the western TP and an anticyclonic circulation anomaly at the heating center.

(<http://ccrc.iap.ac.cn/resource/detail?id=228>). CESM2 model code is available at CESM Project (2025). The figures in this manuscript are prepared using Python software (URL: <https://github.com/python/cpython>).

Acknowledgments

This paper was supported by the National Natural Science Foundation of China (Grant U2442207), the Youth Innovation Promotion Association of Chinese Academy of Sciences (Grant 2021427), the West Light Foundation (xbzg-zdsys202409) of the Chinese Academy of Sciences, Key talent project in Gansu and Central Guidance Fund for Local Science and Technology Development Projects in Gansu (Grant 24ZYQA031).

References

- Bai, W., Chen, X., Tang, Y., He, Y., & Zheng, Y. (2019). Temporal and spatial changes of soil moisture and its response to temperature and precipitation over the Tibetan Plateau. *Hydrological Sciences Journal*, 64(11), 1370–1384. <https://doi.org/10.1080/02626667.2019.1632459>
- CESM Project. (2025). Community Earth System Model (CESM), April 2, 2020 release (version 2.2.0) [Software]. <https://github.com/ESCOMP/CESM>
- Chen, F., Xie, T., Yang, Y., Chen, S., Chen, F., Huang, W., & Chen, J. (2023). Discussion of the “warming and wetting” trend and its future variation in the drylands of Northwest China under global warming. *Science China Earth Sciences*, 66(6), 1241–1257. <https://doi.org/10.1007/s11430-022-1098-x>
- Danabasoglu, G., Lamarque, J., Bacmeister, J., Bailey, D. A., DuVivier, A. K., Edwards, J., et al. (2020). The Community Earth System Model Version 2 (CESM2). *Journal of Advances in Modeling Earth Systems*, 12(2), e2019MS001916. <https://doi.org/10.1029/2019MS001916>
- Ding, Y., Liu, Y., Xu, Y., Wu, P., Xue, T., Wang, J., et al. (2023). Regional responses to global climate change: Progress and prospects for trend, causes, and projection of climatic warming-wetting in Northwest China (in Chinese). 38, 551–562. <https://doi.org/10.11867/j.issn.1001-8166.2023.027>
- Douville, H., Conil, S., Tyteca, S., & Voldoire, A. (2007). Soil moisture memory and West African monsoon predictability: Artefact or reality? *Climate Dynamics*, 28(7), 723–742. <https://doi.org/10.1007/s00382-006-0207-8>
- Duan, A., Wang, M., Lei, Y., & Cui, Y. (2013). Trends in summer rainfall over China associated with the Tibetan Plateau sensible heat source during 1980–2008. *Journal of Climate*, 26(1), 261–275. <https://doi.org/10.1175/JCLI-D-11-0069.1>
- Fang, J., & Yang, X.-Q. (2016). Structure and dynamics of decadal anomalies in the wintertime midlatitude North Pacific ocean–atmosphere system. *Climate Dynamics*, 47(5), 1989–2007. <https://doi.org/10.1007/s00382-015-2946-x>
- Grimm, A. M., Pal, J. S., & Giorgi, F. (2007). Connection between spring conditions and peak summer monsoon rainfall in South America: Role of soil moisture, surface temperature, and topography in Eastern Brazil. *Journal of Climate*, 20(24), 5929–5945. <https://doi.org/10.1175/2007JCLI1684.1>
- Hahn, D. G., & Manabe, S. (1975). The role of mountains in the South Asian monsoon circulation. *Journal of the Atmospheric Sciences*, 32(8), 1515–1541. [https://doi.org/10.1175/1520-0469\(1975\)032<1515:TROMIT>2.0.CO;2](https://doi.org/10.1175/1520-0469(1975)032<1515:TROMIT>2.0.CO;2)
- Han, Y., Jiang, D., Si, D., Ma, Y., & Ma, W. (2024). Time-lagged effects of the spring atmospheric heat source over the Tibetan Plateau on summer precipitation in Northeast China during 1961–2020: Role of soil moisture. *Advances in Atmospheric Sciences*, 41(8), 1527–1538. <https://doi.org/10.1007/s00376-023-2363-8>
- Huang, J., Zhou, X., Wu, G., Xu, X., Zhao, Q., Liu, Y., et al. (2023). Global climate impacts of land-surface and atmospheric processes over the Tibetan Plateau. *Reviews of Geophysics*, 61(3), e2022RG000771. <https://doi.org/10.1029/2022RG000771>
- Japan Meteorological Agency/Japan. (2013). JRA-55: Japanese 55-year reanalysis, monthly means and variances (updated irregularly) [Dataset]. *Research Data Archive at the National Center for Atmospheric Research, Computational and Information Systems Laboratory*. <https://doi.org/10.5065/D60G3H5B>
- Kitoh, A. (2004). Effects of mountain uplift on East Asian summer climate investigated by a coupled atmosphere–ocean GCM. *Journal of Climate*, 17(4), 783–802. [https://doi.org/10.1175/1520-0442\(2004\)017<0783:EMOUOE>2.0.CO;2](https://doi.org/10.1175/1520-0442(2004)017<0783:EMOUOE>2.0.CO;2)
- Kobayashi, S., Ota, Y., Harada, Y., Ebita, A., Moriya, M., Onoda, H., et al. (2015). The JRA-55 reanalysis: General specifications and basic characteristics. *Journal of the Meteorological Society of Japan. Ser. II*, 93(1), 5–48. <https://doi.org/10.2151/jmsj.2015-001>
- Li, R., Bao, H., Li, K., & Chenghai, W. (2016). The memory and climate effects of global soil moisture. *Journal of Glaciology and Geocryology*, 38(6), 1470–1481. <https://doi.org/10.7522/j.issn.1000-0240.2016.0172>
- Li, R., & Wang, C. (2020). Precipitation recycling using a new evapotranspiration estimator for Asian-African arid regions. *Theoretical and Applied Climatology*, 140(1), 1–13. <https://doi.org/10.1007/s00704-019-03063-9>
- Lin, Z., Zuo, Z., Wang, H., You, Q., Xiao, D., Zhang, K., & Qiao, L. (2023). Role of winter soil moisture in subsequent summer thermal anomalies on the Tibetan Plateau. *Journal of Climate*, 36(14), 4739–4753. <https://doi.org/10.1175/JCLI-D-22-0905.1>
- Liu, Y., & Sun, J. (2024). How does the East Siberian sea ice affect the June drought over Northwest China after 2000? *Journal of Geophysical Research: Atmospheres*, 129(20), e2024JD041290. <https://doi.org/10.1029/2024JD041290>
- Liu, Y., Wu, G., Liu, H., & Liu, P. (1999). The effect of spatially nonuniform heating on the formation and variation of subtropical high part III: CONDENSATION heating and south Asia high and western pacific subtropical high. *Acta Meteorologica Sinica* (5), 525–538. <https://doi.org/10.11676/qxb1999.051>
- Lu, M., Yang, S., Li, Z., He, B., He, S., & Wang, Z. (2018). Possible effect of the Tibetan Plateau on the “upstream” climate over West Asia, North Africa, South Europe and the North Atlantic. *Climate Dynamics*, 51(4), 1485–1498. <https://doi.org/10.1007/s00382-017-3966-5>
- Lu, M., Yang, S., Wang, J., Wu, Y., & Jia, X. (2021). Response of regional Asian summer monsoons to the effect of reduced surface Albedo in different Tibetan plateau domains in idealized model experiments. *Journal of Climate*, 34(17), 7023–7036. <https://doi.org/10.1175/JCLI-D-20-0500.1>
- Luo, H., Yu, H., Hu, Z., Zhou, J., Zhang, B., Yang, Y., et al. (2024). Impact of the summer atmospheric heat source over the Tibetan Plateau on interannual variability of meridional circulation on the North side of the Tibetan plateau. *Journal of Climate*, 37(13), 3543–3561. <https://doi.org/10.1175/JCLI-D-23-0599.1>
- Namias, J. (1959). Recent seasonal interactions between north Pacific waters and the overlying atmospheric circulation. *Journal of Geophysical Research (1896–1977)*, 64(6), 631–646. <https://doi.org/10.1029/JZ064i006p00631>
- North, G. R., Bell, T. L., Cahalan, R. F., & Moeng, F. J. (1982). Sampling errors in the estimation of empirical orthogonal functions. *Monthly Weather Review*, 110(7), 699–706. [https://doi.org/10.1175/1520-0493\(1982\)110<0699:SEITEO>2.0.CO;2](https://doi.org/10.1175/1520-0493(1982)110<0699:SEITEO>2.0.CO;2)
- Quesada, B., Vautard, R., Yiou, P., Hirschi, M., & Seneviratne, S. I. (2012). Asymmetric European summer heat predictability from wet and dry southern winters and springs. *Nature Climate Change*, 2(10), 736–741. <https://doi.org/10.1038/nclimate1536>
- Rahmati, M., Amelung, W., Brogi, C., Dari, J., Flammini, A., Bogena, H., et al. (2024). Soil moisture memory: State-of-the-Art and the way forward. *Reviews of Geophysics*, 62(2), e2023RG000828. <https://doi.org/10.1029/2023RG000828>
- Seneviratne, S. I., Corti, T., Davin, E. L., Hirschi, M., Jaeger, E. B., Lehner, I., et al. (2010). Investigating soil moisture–climate interactions in a changing climate: A review. *Earth-Science Reviews*, 99(3), 125–161. <https://doi.org/10.1016/j.earscirev.2010.02.004>

- Shang, W., Duan, K., Ren, X., Guo, Y., Guan, W., & Li, S. (2022). Changes in the dominant mode of summer precipitation over the central-eastern Tibetan Plateau around the mid-1990s. *Journal of Geophysical Research: Atmospheres*, 127(23), e2022JD036617. <https://doi.org/10.1029/2022JD036617>
- Sud, Y. C., Shukla, J., & Mintz, Y. (1988). Influence of land surface roughness on atmospheric circulation and precipitation: A sensitivity study with a general circulation model. *Journal of Applied Meteorology and Climatology*, 27(9), 1036–1054. [https://doi.org/10.1175/1520-0450\(1988\)027<1036:IOLSRO>2.0.CO;2](https://doi.org/10.1175/1520-0450(1988)027<1036:IOLSRO>2.0.CO;2)
- Takaya, K., & Nakamura, H. (2001). A formulation of a phase-independent wave-activity flux for stationary and migratory quasigeostrophic eddies on a zonally varying basic flow. *Journal of the Atmospheric Sciences*, 58(6), 608–627. [https://doi.org/10.1175/1520-0469\(2001\)058<0608:AFOAPI>2.0.CO;2](https://doi.org/10.1175/1520-0469(2001)058<0608:AFOAPI>2.0.CO;2)
- Wang, C., Wang, Z., & Cui, Y. (2009). Spatial distributions and interannual variations of snow cover over China in the last 40 years. *Sciences in Cold and Arid Regions*, 1(6), 509–518. <https://api.semanticscholar.org/CorpusID:13377865>
- Wang, C., Yang, K., & Zhang, F. (2020). Impacts of soil freeze–thaw process and snow melting over Tibetan Plateau on Asian summer monsoon system: A review and perspective. *Frontiers in Earth Science*, 8. <https://doi.org/10.3389/feart.2020.00133>
- Wang, Z., Yang, K., Zhang, F., Zhang, J., & Sun, X. (2023). Impacts of Tibetan Plateau spring snowmelt on spring and summer precipitation in Northwest China. *Atmosphere*, 14(3), 466. <https://doi.org/10.3390/atmos14030466>
- Wu, G., Duan, A., Liu, Y., Mao, J., Ren, R., Bao, Q., et al. (2014). Tibetan plateau climate dynamics: Recent research progress and outlook. *National Science Review*, 2(1), 100–116. <https://doi.org/10.1093/nsr/nwu045>
- Wu, G., Guan, Y., Liu, Y., Yan, J., & Mao, J. (2012). Air-sea interaction and formation of the Asian summer monsoon onset vortex over the Bay of Bengal. *Climate Dynamics*, 38(1), 261–279. <https://doi.org/10.1007/s00382-010-0978-9>
- Wu, G., Liu, Y., He, B., Bao, Q., Duan, A., & Jin, F.-F. (2012). Thermal controls on the Asian summer monsoon. *Scientific Reports*, 2(1), 404. <https://doi.org/10.1038/srep00404>
- Wu, G., Liu, Y., Zhang, Q., Duan, A., Wang, T., Wan, R., et al. (2007). The influence of mechanical and thermal forcing by the Tibetan Plateau on Asian climate. *Journal of Hydrometeorology*, 8(4), 770–789. <https://doi.org/10.1175/JHM609.1>
- Wu, G., & Zhang, Y. (1998). Tibetan plateau forcing and the timing of the monsoon onset over south Asia and the South China sea. *Monthly Weather Review*, 126(4), 913–927. [https://doi.org/10.1175/1520-0493\(1998\)126<0913:TPFATT>2.0.CO;2](https://doi.org/10.1175/1520-0493(1998)126<0913:TPFATT>2.0.CO;2)
- Wu, G.-X. (1984). The nonlinear response of the atmosphere to large-scale mechanical and thermal forcing. *Journal of the Atmospheric Sciences*, 41(16), 2456–2476. [https://doi.org/10.1175/1520-0469\(1984\)041<2456:TNROTA>2.0.CO;2](https://doi.org/10.1175/1520-0469(1984)041<2456:TNROTA>2.0.CO;2)
- Wu, J., & Gao, X. (2013). A gridded daily observation dataset over China region and comparison with the other datasets. *Chinese Journal of Geophysics*, 56(4), 1102–1111. <https://doi.org/10.6038/cjg20130406>
- Xie, Y., Huang, J., Wu, G., Liu, Y., Dong, W., Lu, M., et al. (2023). Oceanic repeaters boost the global climatic impact of the Tibetan Plateau. *Science Bulletin*, 68(19), 2225–2235. <https://doi.org/10.1016/j.scib.2023.07.019>
- Xu, X., Zhou, M., Chen, J., Bian, L., Zhang, G., Liu, H., et al. (2002). A comprehensive physical pattern of land-air dynamic and thermal structure on the Qinghai-Xizang Plateau. *Science in China - Series D: Earth Sciences*, 45(7), 577–594. <https://doi.org/10.1360/02yd9060>
- Yang, K., & Wang, C. (2019). Seasonal persistence of soil moisture anomalies related to freeze–thaw over the Tibetan Plateau and prediction signal of summer precipitation in eastern China. *Climate Dynamics*, 53(3), 2411–2424. <https://doi.org/10.1007/s00382-019-04867-1>
- Yang, K., Wang, C., & Bao, H. (2016). Contribution of soil moisture variability to summer precipitation in the Northern Hemisphere. *Journal of Geophysical Research: Atmospheres*, 121(20), 12–124. <https://doi.org/10.1002/2016JD025644>
- Yuan, Y., Lai, X., Gong, Y., & Chen, J. (2021). The impacts of late spring soil moisture in the Tibetan Plateau on summer precipitation in eastern China. *International Journal of Climatology*, 41(2), 862–877. <https://doi.org/10.1002/joc.6692>
- Zha, P., & Wu, Z. (2023). Contribution of the Tibetan plateau snow cover to the record-breaking rainfall over the Yangtze River valley in June 2020. *Atmosphere-Ocean*, 61(2), 122–134. <https://doi.org/10.1080/07055900.2022.2151408>
- Zhang, Q., Lin, J., Liu, W., & Han, L. (2019). Precipitation seesaw phenomenon and its formation mechanism in the eastern and western parts of Northwest China during the flood season. *Science China Earth Sciences*, 62(12), 2083–2098. <https://doi.org/10.1007/s11430-018-9357-y>
- Zhang, R., & Zuo, Z. (2011). Impact of spring soil moisture on surface energy balance and summer monsoon circulation over East Asia and precipitation in East China. *Journal of Climate*, 24(13), 3309–3322. <https://doi.org/10.1175/2011JCLI4084.1>
- Zhao, Y., Li, R., Yang, X., He, D., & Zhang, C. (2013). Impact of the anomaly of surface sensible heat in Qinghai-Xizang plateau and its surrounding areas on summertime precipitation in northern Xinjiang. *Plateau Meteorology*, 32(5), 1215–1223. <https://doi.org/10.7522/j.issn.1000-0534.2012.00117>
- Zhou, J., Wen, J., Liu, R., Wang, X., & Xie, Y. (2018). Late spring soil moisture variation over the Tibetan Plateau and its influences on the plateau summer monsoon. *International Journal of Climatology*, 38(12), 4597–4609. <https://doi.org/10.1002/joc.5723>
- Zhou, L.-T., & Huang, R.-H. (2010). Interdecadal variability of summer rainfall in Northwest China and its possible causes. *International Journal of Climatology*, 30(4), 549–557. <https://doi.org/10.1002/joc.1923>
- Zhu, C., Ullah, W., Wang, G., Lu, J., Li, S., Feng, A., et al. (2023). Diagnosing potential impacts of Tibetan Plateau spring soil moisture anomalies on summer precipitation and floods in the Yangtze River Basin. *Journal of Geophysical Research: Atmospheres*, 128(8). <https://doi.org/10.1029/2022JD037671>
- Zhu, X., Yang, M., Liu, G., Liu, Y., Li, W., Nan, S., & Sun, L. (2023). A precursory signal of June–July precipitation over the Yangtze River Basin: December–January tropospheric temperature over the Tibetan Plateau. *Advances in Atmospheric Sciences*, 40(11), 1986–1997. <https://doi.org/10.1007/s00376-022-2079-1>